Numerical Modelling of unilateral point-focusing electromagnetic acoustic transducer with experimental validation

Hongyu Sun[a], Shen Wang[a], Songling Huang [a,*], Qing Wang[b], and Wei Zhao[a]

a State Key Lab of Power System, Department of Electrical Engineering, Tsinghua University, Bejing, China

b Department of Engineering, Durham University, Durham, United Kingdom

Abstract— Electromagnetic ultrasonic testing, based on the propagation characteristics of the ultrasonic wave in the medium, is an effective technique for defect detection. The structural of the electromagnetic acoustic transducer (EMAT) determines the detection effect, which should be reasonably designed. We propose an improved unilateral point-focusing EMAT structure with curved coils in this manuscript. The 3D model of the designed EMAT is numerically simulated utilizing the finite element method, and the bilateral point-focusing EMAT is also studied for comparison. The simulation results of the magnetic field intensity and the distributions of the displacement are shown in the manuscript, which prove the effectiveness of the improved unilateral point-focusing EMAT. Five impact parameters such as aperture angle, focal position, excitation current, lift-off distance, and coil winding number are investigated in detail. We verify the calculation results of the aperture angle and excitation current by the experiments. The conclusion shows that the focusing intensity of the improved unilateral point-focusing EMAT is relatively higher, and other factors also have a significant effect on the focal intensity.

Keywords: Point–focusing, Electromagnetic acoustic transducer (EMAT), unilateral, bilateral, numerical simulation

1. Introduction

Electromagnetic ultrasonic detection technique, as one of the ultrasonic nondestructive testing (NDT) technologies, has significant advantages on detecting cracks, interlayers, and folds on the surface of the material that caused by fatigue, aging and thermal expansion [1–3]. Due to the dispersion characteristics of the ultrasonic guided waves and the characteristics of different modes, it is necessary to consider the performance of the material to select an appropriate ultrasonic guided wave mode for the inspection. As an ultrasonic guided wave excitation and receiving transducer, the electromagnetic acoustic transducer (EMAT) relies on the electromagnetic coupling to realize the wave propagation [4–8]. The types of waves produced by the EMATs are distinguished according to the vibration direction and the direction of the wave propagation in an elastic medium, which can be divided into the longitudinal wave, shear wave, surface wave and plate wave [9–11].

* Corresponding author: Songling Huang, State Key Lab of Power System, Department of Electrical Engineering, Tsinghua University, Beijing 100084, China. Email: huangsling@tsinghua.edu.cn

There are some advantages for the EMAT such as no coupling medium required, high speed and temperature available. EMAT is the core component of the electromagnetic ultra-sonic testing system. However, its weak transduction efficiency and the broad radiation patterns of elastic waves reduce the energy of ultrasonic signals [12–16]. Moreover, the elastic waves generated by the EMAT propagate in nearly all the directions in the specimen, which further reduces the energy of the detected ultrasonic signal. Therefore, the energy concentration of the ultrasonic wave is a critical issue and has been highly concern by researchers and engineers.

Thring et al. developed a method to detect the defects on the surface of materials by focusing the Rayleigh waves [17,18]. The method improves the efficiency of the energy conversion of the electromagnetic-acoustic and makes it easier to detect small defects on the specimen's surface. The focusing method of the surface waves is not applicable for internal defect detection. Therefore, the focusing method for bulk waves (especially the SV waves) has been developed to improve the detection accuracy of the internal defects. As for the focusing method of the SV waves, Ogi developed a sharp direction line-focusing EMAT by changing the spacings between the contiguous excitation coils, so the propagation direction of the SV waves can be focused on a focal line [19]. Then he realized that only the directional SV wave focusing method was incomplete as the condition of the equal phase (coherency) was not satisfied. Therefore, he improved the line focusing method of the SV waves and the waves radiated by each coil focused on a line in the same phase [20]. However, as the line focusing is one of the energy concentration forms in the 2D plane, it is difficult to determine the spatial shape and the location of the defects in the 3D region. Then the point-focusing method was proposed by Takishita, and he utilized the curved meander line coils to focus the SV waves on a point within the space [21–23]. The detection accuracy and signal resolution of the SV waves are further improved. However, Due to the symmetrical structure of the transducer, the SV waves generally propagate in both directions of the specimen. In the measurement, attention is usually paid to whether there is a defect in a specific direction or a point in general. The wave propagating along the unconcerned side makes it difficult to identify the signal of the SV waves and extract them from the noise. Therefore, it is necessary to focus the guided wave signal to a certain side and suppress the signal on the other side.

In recent years, due to the rapid development of computer technology, the numerical simulation method has been widely used with its significant advantages. The finite element method and commercial numerical simulation software are utilized in various fields such as physical modeling,

chemical reactions, and bioengineering. Therefore, to calculate the characteristics of EMAT, the numerical simulation method has been widely used [24–29]. As for commercial software, COMSOL shows extreme accuracy and convergence compared with other software [30]. By using the COMSOL Multiphysics, the EMATs in steady-state, transient-state and frequency domain were fully simulated and explained by Wang et al. and the modeling process of the EMAT was also explained in his paper [31]. He proposed a simulation method based on the Lorentz force EMAT by COMSOL, but it still has difficulties in calculating 3D problems. There are many simulations of SV waves in recent years, and point-focusing EMATs are simulated by Jia et al. at different aperture angles and focal offsets [32]. He obtained the point focusing of the SV wave through simulation but did not achieve the unilateral focusing of the SV wave so that it may cause the mutual influence of the bilateral SV waves. Wang et al. developed a new design of the coils for unilateral line-focusing SV wave EMATs and focusing Rayleigh waves [33]. However, he only realized the unilateral focusing method in the 2D space, which is not sufficient enough for the wave focusing. Therefore, their methods shown above can be further improved in this manuscript.

A 3-D numerical simulation on the EMAT is achieved by utilizing finite element & multi-physical field methods in this manuscript. The magnetostatics field and bulk wave propagation are investigated by solving the electromagnetic model and the elasto-dynamic model. The bilateral and unilateral point focusing EMATs are designed and calculated as a particular case. The bilateral EMAT uses just one meander line coil with an aperture angle while the unilateral EMAT utilizes dual-channel spacing-variable coils. The effects of the aperture angle, focal position, excitation current, lift-off distance, and coil winding number are investigated in the simulation. Moreover, the results of the numerical simulation are verified by the experiments.

2. Unilateral point-focusing EMAT design

SV waves, which also named the bulk waves, are excited in the plate and usually propagate along

two symmetrically inclined directions with sharp directivity. To achieve a better beam focusing effect, a variable meander line coil under a vertical bias magnetic field is utilized to generate the focusing SV waves. The unilateral point-focusing EMAT is designed in this manuscript to improve the focusing ability of the SV waves, and the configuration is shown in Fig. 1(a). It can be seen from the figure that the phase shift of the excitation current between coil A and coil B is 90°.

Moreover, the coils are designed to weaken the SV waves on the other side of the focal point, which reduce the interference of those signals. The permanent magnet above the aluminum specimen provides the vertical bias magnetic field for the excitation of the Lorentz force. The magnetostriction effect is not considered in this study because the specimen is non-ferromagnetic [34]. The curved coils with continuously changing spaces are utilized to generate the point-focusing SV waves.

Figure 1(b) shows the 2D schematic diagram of the unilateral point-focusing EMAT. The N pole of the permanent magnet placed down near the surface of the aluminum. Since the coil excitation current is applied periodically, the skin depth layer of the aluminum plate will induce the eddy currents correspondingly. The cross-sections of the meander line coils are expressed as $x_1, x_2, \ldots, x_i,$ respectively. The focal point is determined first, and the coordinate is defined as (0, 0) in the figure. The distances from each source to the focal point are $r_1, r_2, \ldots, r_i$, respectively.

Research methods of the focusing EMAT are developed by Ogi et al., and the major radiation angle φ that obtained from the phase-matching theory is shown in Fig. 1(b). The angle φ is determined the spacing l_i, the wave velocity c and the frequency f of the pulsed current in the coil [12].

$$\sin\varphi = \frac{c}{2lf}. \tag{1}$$

Moreover, the position of the meander line coil can be calculated by the following equation:

$$\sin\varphi_i = \frac{c_S}{2l_i f} = \frac{|R\sin\varphi - x_i - l_i/2|}{\sqrt{(R\cos\varphi)^2 + (R\sin\varphi - x_i - l_i/2)^2}}. \tag{2}$$

However, this directional focusing method can only ensure the focusing path of the beam and cannot guarantee the coherency of the wave phases. Therefore, the coil position should be designed specifically. The design steps of the coil position are as follows. First, the excitation current amplitude and frequency of the coil are determined. Then, the position of the focal point and the first coil x1 are selected. Since the radiation angle of the SV wave reaches its maximum at around 30°, the radiation angle of as many coils as possible needs to be ensured at around 30° during the coil design. In the bilateral point-focusing EMAT, the spacing between the coils generally satisfies the following formula

$$r_i - r_{i+1} = \frac{c}{2f} = \frac{\lambda}{2}, \tag{3}$$

where λ is the wavelength of the SV wave.

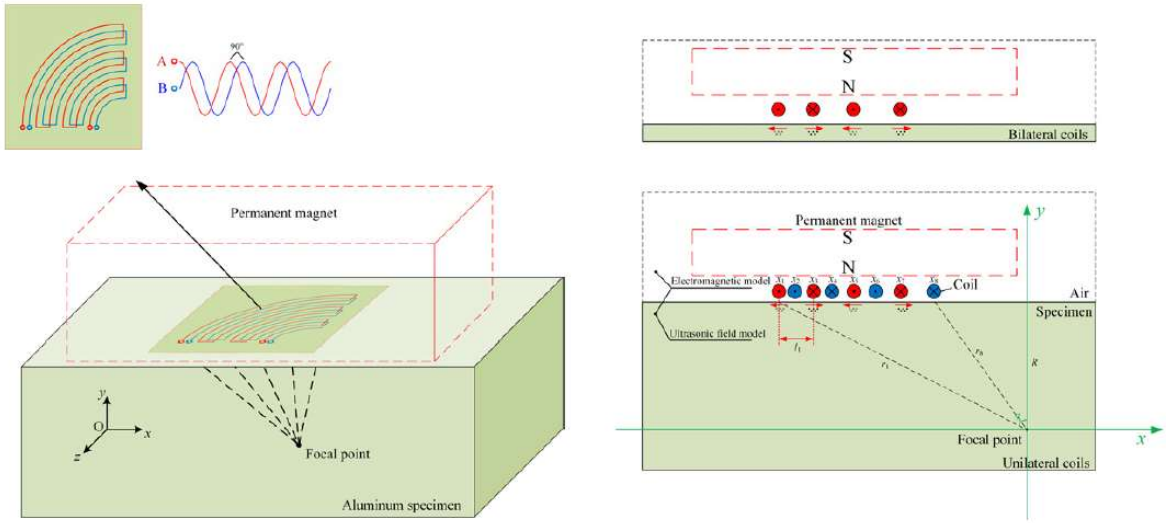

Fig. 1. Configuration of the unilateral point-focusing EMAT: (a) 3D. (b) 2D cross section.

For the unilateral point-focusing EMAT coils in this manuscript, the coil spacing should satisfy the following formula

$$r_i - r_{i+1} = \frac{c}{4f} = \frac{\lambda}{4}. \tag{4}$$

It should be noted that the phase shift between the excitation currents of the adjacent coils is 90°, such as coil A and coil B in this study. Both of the bilateral and unilateral EMATs are designed to promote the SV waves at the same phase (in the opposite phase on the other side of the focal point for the bilateral EMAT) when it reaches the focal point.

3. Modelling method

The calculation of Lorentz force is solved by the joint-calculation using the AC/DC Module and the magnetic field (no current) module in the manuscript. Moreover, the solid mechanic module with the linear elastic material is utilized to calculate the propagation process of the SV waves. With the coupling of Lorentz force among the various modules, the calculation of each physical field will perform simultaneously and couple to each other.

The configuration of the 3D model in the simulation is shown in Fig. 2, which includes a permanent magnet, coils, an aluminum specimen, air, and free boundaries. It shows that the size

of the specimen is 150 × 150 × 60 mm3. The horizontal distance of the permanent magnet is wide enough to avoid the edge effect of the magnet, and the size of the permanent magnet is 80 × 80 × 10 mm3. To analyze the influence of the various parameters on the focusing effect, some parameters are not set as fixed values in the study. The excitation current is a burst wave with an amplitude of 3.5 A to 6.5 A. The expression of the excitation burst current for the EMAT coils is

$$i(t) = \beta e^{-\alpha(t-\tau)^2} \cos[2\pi f_c(t-\tau)+\theta], \tag{5}$$

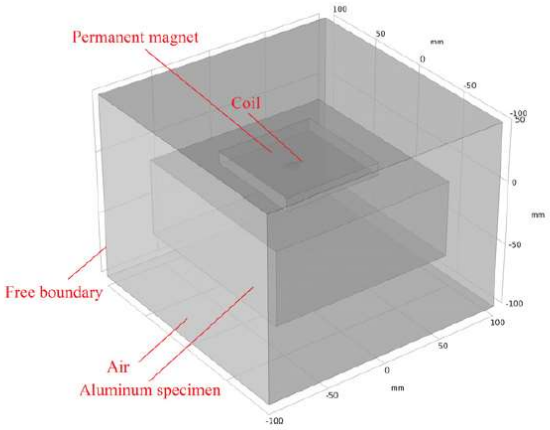

Fig. 2. 3D Configuration of the model in the simulation

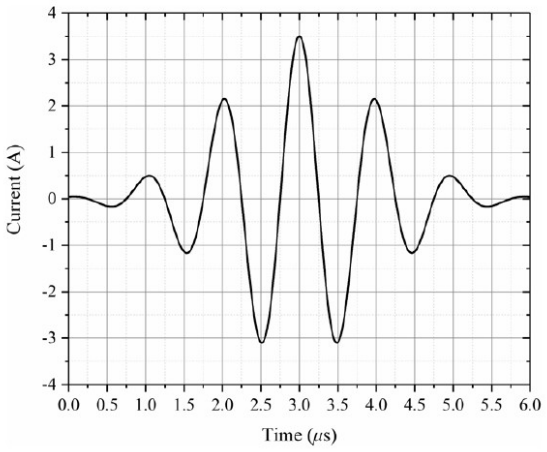

Fig. 3. The waveform of the excitation current

where β is the amplitude of the signal, α is the bandwidth factor, τ is the arrival time, f c is the central frequency, and θ is the phase delay. The value of the parameters above is shown in Table 1, and the waveform of the excitation current is shown in Fig. 3. The aperture angle of the coil is

set at 45°, 90°, 135°, and 180°. The position of the focal point is also investigated in the study. The lift-off distance between the coil and the upper surface of the specimen is from 0.05 mm to 0.25 mm. Moreover, the number of coil winding is set to 1, 2, 3 and 4 in the simulation. Some of the parameter characteristics introduced above have been further analyzed through the experiments. Then other parameters of the point-focusing EMAT are shown in Table 2.

Table 1

Parameters of burst signals for the coils

Parameters	Value
β(A)	3.5
α (s^{-2})	5 x10^{11}
$\tau(\mu s)$	3
fc (MHz)	1
θ (°)	0

Table 2

Parameters of the point-focusing EMAT

Parameters	Value
SV wave velocity(km/s)	3.2
Lame's constants λ (GPa)	58
Lame's constants μ (GPA)	29
Aluminum specimen mass density (kg/m^3)	2832
Aluminum specimen conductivity (S/m)	3.65 x 10^7
Magnetism of the magnet (T)	1.2
Relative permeability of the magnet	400

4. Simulation results

To simulate the bilateral and unilateral point- focusing EMATs under the influence of different parameters, a particular case is given here to explain. The finite element method is utilized in the calculation as discussed above, and a 2D cross-section is selected to analyze the distribution of the

displacement field. Five variables are analyzed in this manuscript, and the effect of each parameter on the focusing ability should be studied by the control variate method.

As a particular case, the aperture angle is set to 90°, the position of the focal point is predetermined, the amplitude of the excitation current is 3.5 A, the lift-off distance is 0.1 mm, and the number of coil winding is 4. It should be noted that the following discussions only change one of the above parameters while keeping others unchanged. The static magnetic field generated by the permanent magnet is calculated in the simulation of the steady-state first, and the distribution of the magnetic field inside the specimen is obtained.

The induced current of the pulse current in the coil is calculated and the Lorenz force at each point inside the specimen can be obtained by taking the calculated magnetostatics field above as the background magnetic field. Then the Lorenz force is applied to the aluminum material, and the stress, strain, and displacement of the specimen are calculated. In the simulation, the receiving transducer has the same structure as the transmitting transducer. As a dimensionless processing method that makes the absolute value of a physical system a relative value, the normalization method is used in this work to achieve easy comparison and avoid errors caused by the signal conversion. The normalized standard is the maximum value of the measured signal. Figure 4(a–d) show the distributions of the displacement field and unilateral point-focusing EMATs. Figure 4(e) shows the relationship between the amplitude of the normalized displacement at the position of the focal point and the time. The detail of Fig. 4(a) represents the simulation results of the surface Rayleigh wave, longitudinal wave, and the shear wave. It can be seen in Fig. 4(e) that the positions of the focal and the radiant point are determined. The moment of the arrival of the longitudinal wave is about 6 μs and that of the SV wave is about 12 μs. This phenomenon can be explained by the fact that the sound velocity of the longitudinal wave in aluminum is twice as large as that of the SV wave. It is clearly shown in the figures that the unilateral point-focusing EMATs possess better beam focusing capabilities, and the amplitude of the unilateral focusing SV wave is enhanced than that of the bilateral one.

Moreover, the SV waves account for a large part of the unilateral EMAT when compared to that of the Rayleigh waves and the longitudinal waves. It is demonstrated in Fig. 4(c–d) that the bilateral focusing EMAT exhibits approximately symmetrical characteristics, while the unilateral

point-focusing EMAT shows the ability to focus the SV waves on the one side and weakened the wave on the other side.

4.1 Aperture angle

The selection of different aperture angles has a significant influence on the amplitude of the signal when the focusing radius is fixed. Therefore, to study the effect of the change of aperture angles on the pointfocusing EMATs, other parameters such as the focal position, exciting current amplitude, lift-off distance and the number of coil winding remain constant. The normalized amplitudes of the signal for different aperture angles are shown in Fig. 5 where Figs. 5(a) and (b) are for the bilateral and unilateral, respectively. It can be seen from the figure that the increase of the aperture angle will increase the amplitude of the signal, and the signals on the left side of the amplitude-distance figure of the unilateral EMAT are also suppressed. To compare the difference between the bilateral and unilateral EMATs, the normalized amplitudes are plotted in the same figure in Fig. 5.

It is shown in Fig. 6 that with the increase of the aperture angle, the difference between the focusing ability of bilateral and unilateral EMATs is increasing. Moreover, the normalized amplitude is approximately proportional to the size of the aperture angle, which can be explained by the fact that an increase in the length of the coil will increase the energy of the wave beam simultaneously.

4.2 Focal position

Point-focusing EMAT was developed by changing the spacing of the meander line so that the SV waves generated from all sources become coherent at the focal point. In most of the previous studies, the focal point was selected first at a fixed frequency, and then the spacing of the meander line coils are adjusted through a specific equation. However, as the initial step of the EMAT design, the selection of the focal point should not be arbitrary at a certain depth. Therefore, the effect of different focal positions on the focusing intensity of the signal is discussed in this manuscript, and the bilateral and unilateral point-focusing EMATs are selected to investigate the effect of the focal position. Then the position of the focal point and the design of the coil are shown in Fig. 7. For comparison analysis, cross-sectional data were extracted for the analysis. Moreover, for a 2D coordinate system, the focal point's coordinate is set to (0,0) in the study. Any change of the focal

position will lead to the redesign of the coil spacing, so we select both the vertical offset and horizontal offset for the analysis. The effect of the horizontal offset of the focal position on the normalized amplitude of the signal is shown in Fig. 8(a) and the result for the vertical offset is shown in Fig. 8(b).

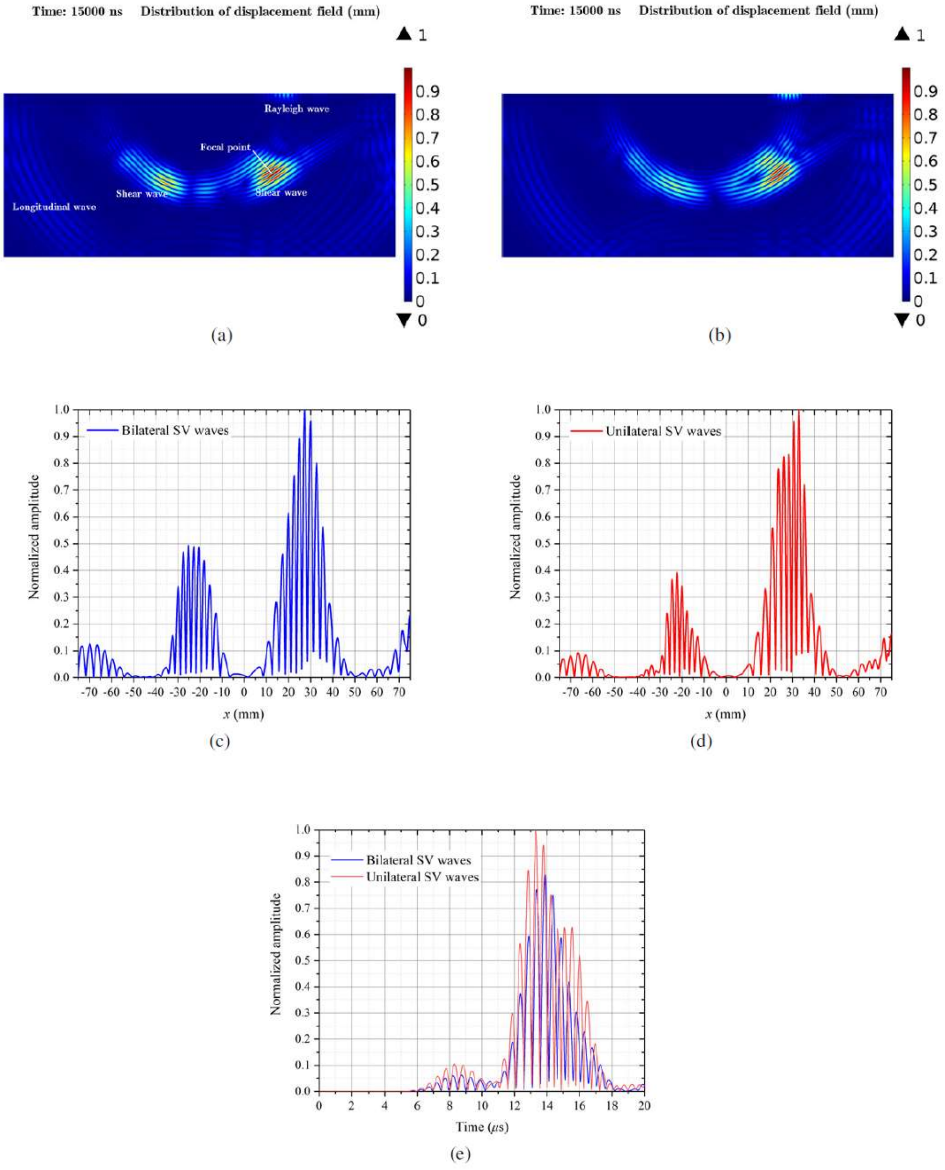

Fig. 4. The simulation results for the particular case at 6μs: (a) The distribution of the displacement field for bilateral line-focusing EMAT.(b) The distribution of the displacement field for unilateral line-focusing EMAT. (c) Normalized amplitude of the displacement field along the horizontal direction for bilateral line-focusing EMAT. (d) Normalized amplitude of the displacement field along the horizontal direction for unilateral line-focusing EMAT. (e) The relationship between the amplitude of the normalized displacement at the position of the focal point and the time.

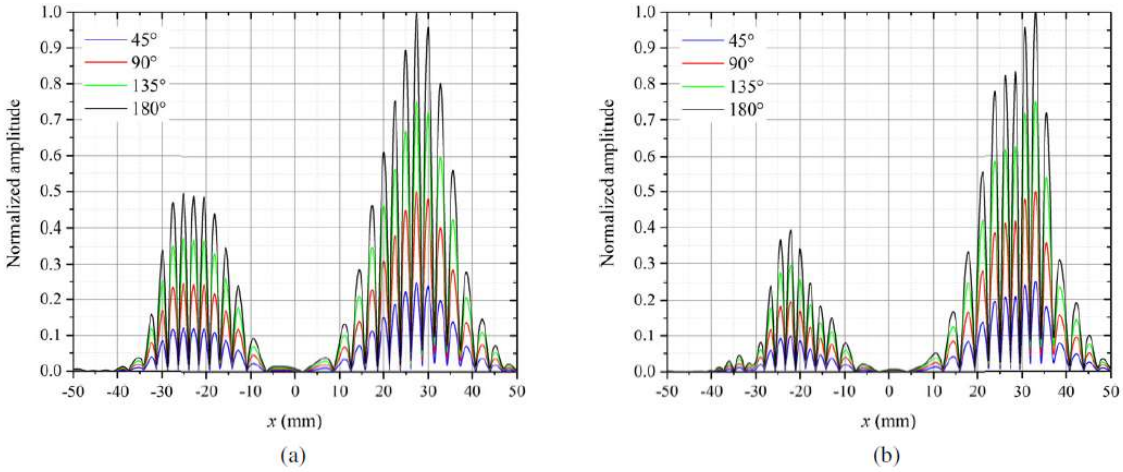

Fig. 5. Normalized amplitude of the displacement field of different aperture angles for point-focusing EMAT: (a) Bilateral point-focusing EMAT. (b) Unilateral point-focusing EMAT.

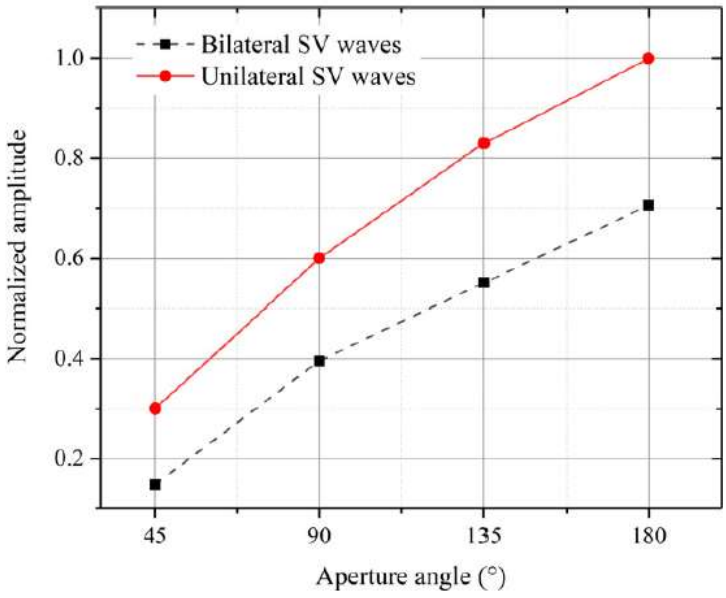

Fig. 6. Normalized amplitudes of the displacement field at different aperture angles for bilateral and unilateral point-focusing EMATs.

Figure 8(a) shows that the normalized amplitude of the signal decreases with the increase of the horizontal offset, and the amplitudes of the unilateral SV waves are larger than that of the bilateral SV waves. It is known that the amplitude of the SV waves attenuates as their propagation distance

increases, but the signal attenuation is reduced as the focal point moves towards the meander line coils. It can be seen in Fig. 8(b) that the relationship between normalized amplitude and vertical offset is not linear. The amplitude reaches its peak at the vertical offset of −5 mm while it decreases when the offset is −10 mm. It is known that the amplitude directivity reaches its peak when the radiation angle is around 30°, and the amplitude of the SV wave will drop sharply when the radiation angle exceeds 30° [19,20,35]. Therefore, due to the obliquely incident properties and energy concentration properties of the SV waves, the nonlinear relationship in Fig. 8(b) can be explained.

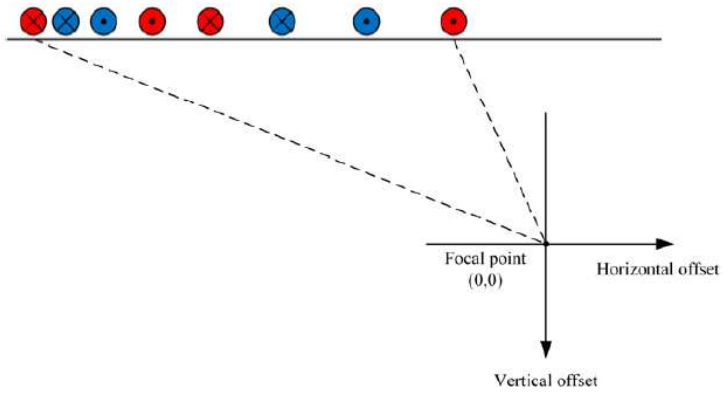

Fig. 7. The arrangement of the meander line coil and the position of the focal point.

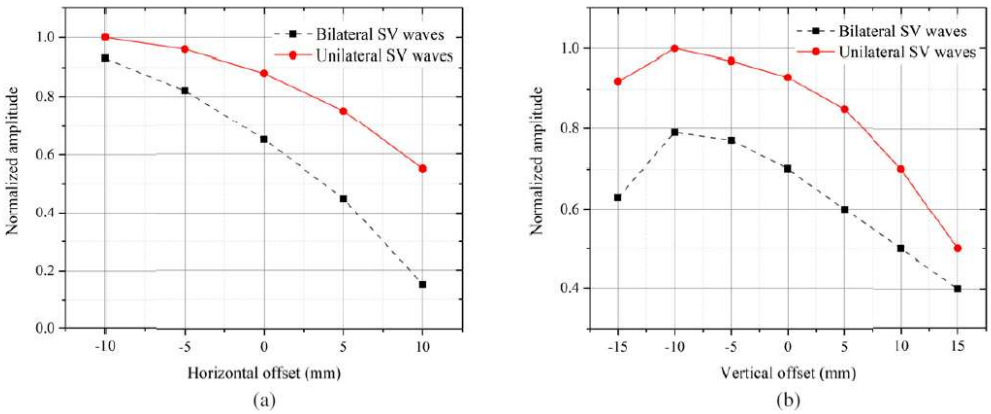

Fig. 8. Normalized amplitudes of the displacement filed at the different focal position for the bilateral and unilateral line-focusing EMATs: (a) The effect of the horizontal offset. (b) The effect of the vertical offset.

4.3 Excitation current

Excitation current, as a driving source for the point-focusing EMAT, has a great influence on the properties of the SV wave. Therefore, it is necessary to analyze the characteristics of the excitation current in the study. As described above, the waveform of the excitation current is a burst wave, and the frequency is fixed into 1 MHz. Figure 9 shows the relationship between the normalized amplitude and the excitation current.

It can be seen from Fig. 9 that as the excitation current amplitude increases, the normalized amplitude of the signal also increases, and there is a parabolic relationship between them. It can be observed that as the current amplitude increases, the focusing intensity of the unilateral point-focusing EMAT becomes stronger when compared to the bilateral point-focusing EMAT. This is because, for the burst signal, the change in the peak value of the excitation current also affects the secondary peak, so the nonlinearity of Fig. 9 can be interpreted as a nonlinear superposition of the excitation signal. When the excitation current is smaller than 3.5 A, the difference between bilateral and unilateral point-focusing EMATs is not that obvious.

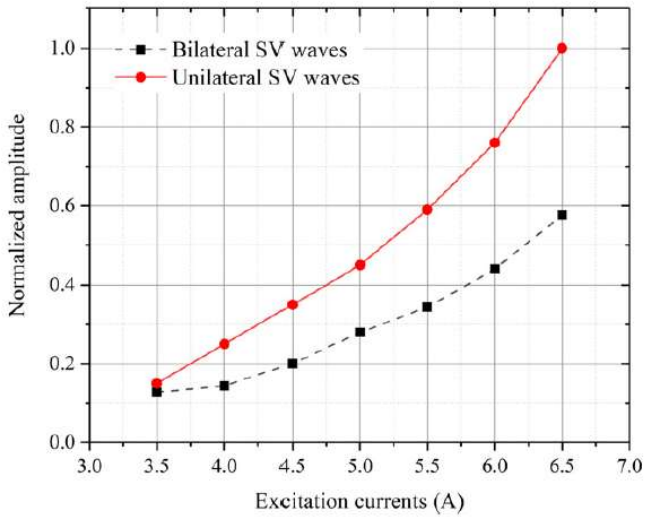

Fig. 9. Effect of the excitation current on the normalized amplitude of the displacement field.

It should be noticed that the characteristics of the burst current are affected by the current parameters shown in Table 1. As the bandwidth factor α, it can be used to change the waveform width of the signal (Fig. 10). Then we study the effects of the selection of different α. It is shown

in the figure that the change of the bandwidth factor α only affects the amplitude of the signal side lobes while the main lobe of the signal is not affected. To investigate the role of the bandwidth factor α in the performance of the new EMATs, simulations with different values of α are performed in COMSOL and the distributions of the displacement field at 15 μs are shown Fig. 11(a–e). It is shown in the figures that the change of the bandwidth factor α has a significant effect on the wave propagation. Figure 12(a–b) shows that the width of the pulse signal decreases as α increases and the amplitude of the signal decreases weakly with the increase of the bandwidth factor α, which is shown in Fig. 13. It proves that the magnitude and waveform of the excitation current need to be well chosen, and that larger currents and smaller bandwidth factors are beneficial for the focusing of the SV waves. Moreover, the amplitude of the ultrasonic wave generated by the burst current excitation is related to the maximum value of the burst signal. Therefore, the waveform shown in Fig. 10 near the peak of the burst current has a large influence on the signal intensity and the focusing effect of the SV wave. Although the pulse signal cannot be eliminated on the non-focusing side, the ultrasonic phase superposition can still be achieved on the focusing side. As the bandwidth factor α decreases, the effect of unilateral focusing will be enhanced, which can be explained by the fact that the waveform of the burst signal becomes more and more similar to the waveform of the sinusoidal signal as α decreases.

4.4 Lift-off distance and the coil winding

The distance from the coil to the surface of the specimen (known as the lift-off distance) as well as the coil winding number, can strongly affect the Lorentz force in the specimen. The effects of the liftoff distance and the coil winding are simulated at different conditions. It is shown in Fig. 14 that the normalized amplitude decreases with the increase of the lift-off distance, and as the lift-off distance increases, the reduced rate of the normalized amplitude decreases. It proves that reducing the lift-off distance will increase the transmission efficiency of the EMAT's energy.

As for the effect of the coil winding number, Figure 15 shows the corresponding relationship. The normalized amplitude of the signal increases with the increase of the coil winding number. It can be found that the contribution of different coils to the amplitude of the focal point is different. The closer to the focal point, the more the coil's contribution. It can be explained that the relative position between the coils and the focal point is of the main influence on the normalized amplitude.

Similar to the results above, the unilateral point-focusing EMATs possess better-focusing performance compared to the bilateral point-focusing EMATs.

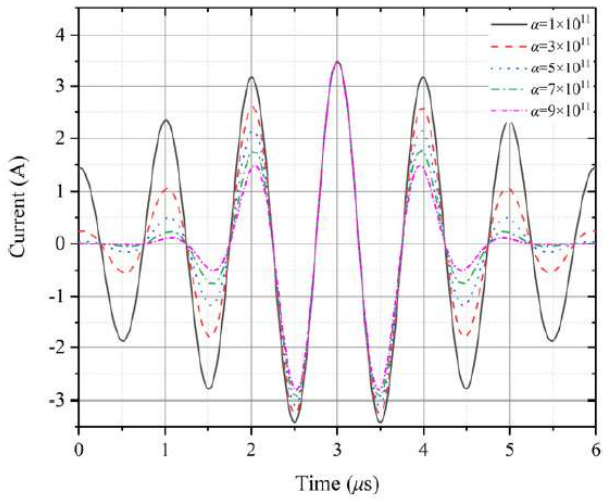

Fig. 10. The waveform of the excitation current with different bandwidth factors

5. Experiment validation

The focusing characteristics are analyzed by the numerical method above to investigate the characteristics of the point-focusing SV waves under different conditions. The experiments verify the validity of the simulation results. Unilateral point-focusing EMATs are utilized in the experiments in this manuscript. The size of the aperture angle and the amplitude of the excitation current can be controlled more accurately, so the amplitude of the signal at different aperture angles and excitation currents are studied through the experiments. The schematic diagram of the experimental setup is shown in Fig. 16.

As the most important source of the signal generation in EMAT, the signal generation and reception in the experiment should be modulated and amplified before being processed. Therefore, RPR-4000 PULSER/RECEIVER is selected in the experiment. To excite two bursts simultaneously, two instruments are utilized in the measurement. The permanent magnet shown in Fig. 16 is of Nd-Fe-B magnet, which size is the same as the geometric structure utilized in the simulation above. The coils inside the transmitter and the receiver are well-designed and made by the PCB method. The material of the specimen is aluminum, and the size is 150 × 150 × 60 mm3 in the experiment, and the coils are excited by a burst current with an amplitude of 3.5 A, frequency

of 1 MHz and bandwidth factor of 5 × 1011, which can be controlled by the RPR-4000 power and the programming method, and the waveform of the output current can be also mentioned.

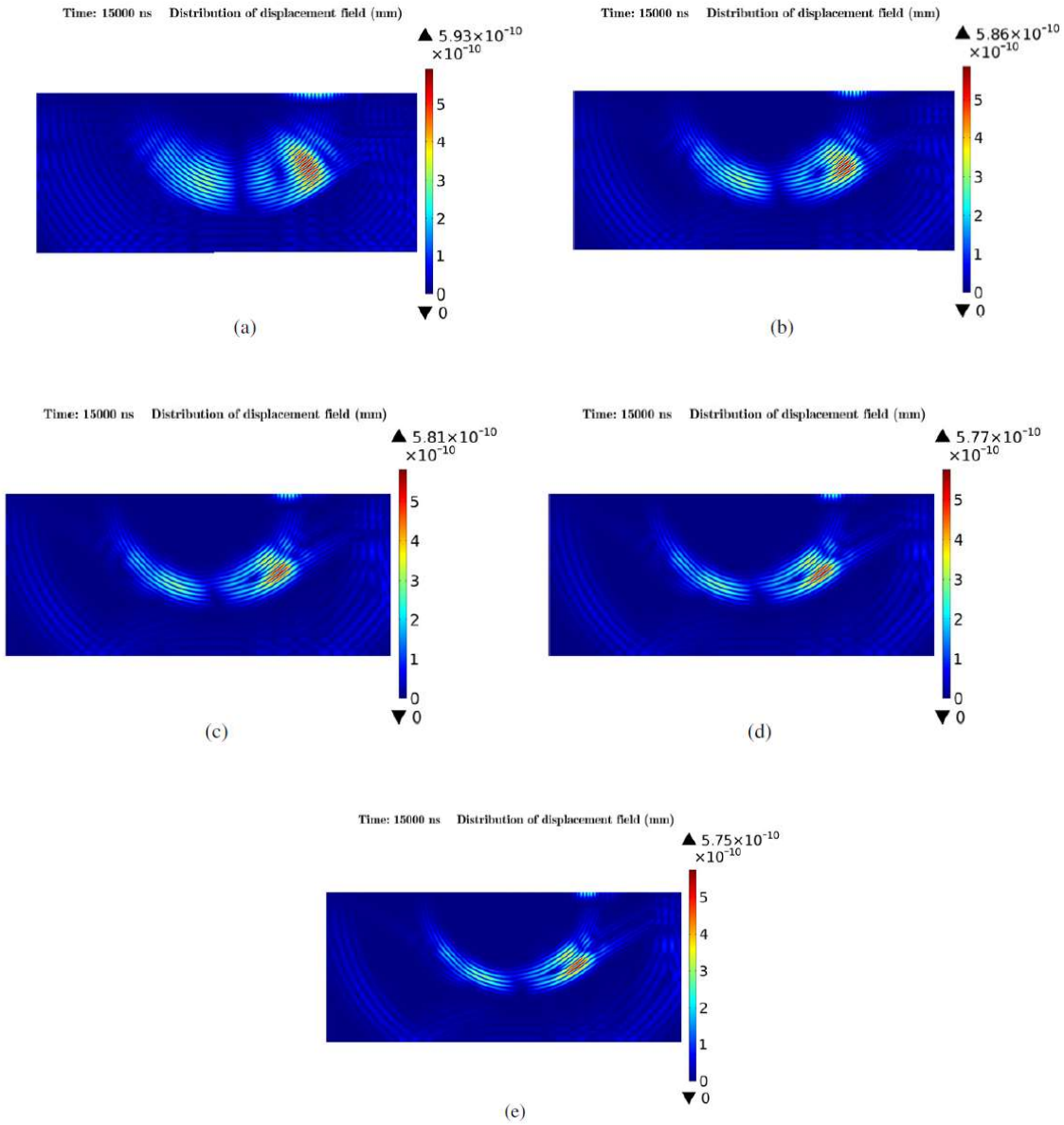

Fig. 11. The distribution of the displacement field at 15μs: (a) α = 1x10^{11}. (b) α = 3x 10^{11}. (c) α =5x1011. (d) α = 7x1011. (e) α =9x10^{11}

The focal point and structures of the transmitter and the receiver are the same, and the experimental conditions are consistent with the simulation conditions. Due to the low energy conversion efficiency of EMAT, high-power pulse current excitation is required. Therefore, to obtain the

maximum output power of the excitation source, it is required to match the impedance of the load with the internal impedance of the excitation source, then 150 ohms matching impedance are utilized in the experiment to improve the accuracy and efficiency of the EMAT.

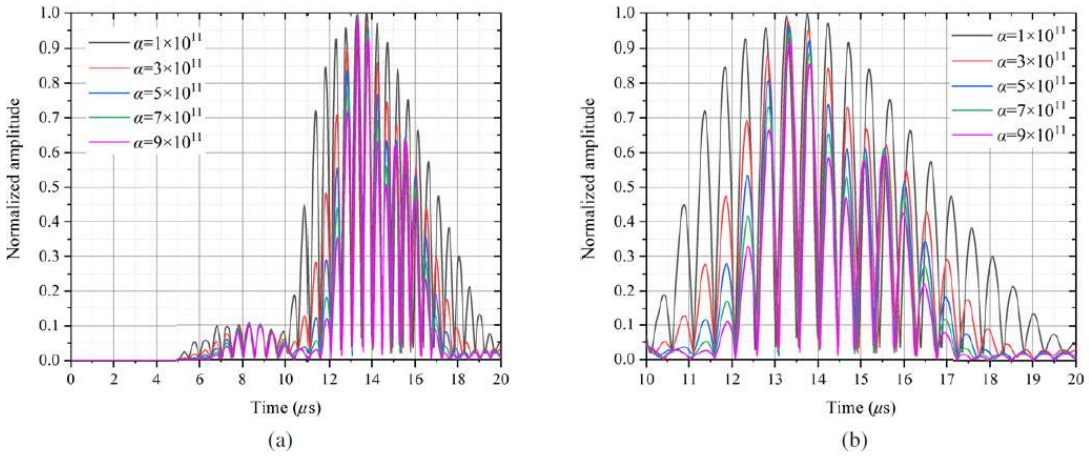

Fig. 12. The relationship between the amplitude of the normalized displacement at the position of the focal point and the time: (a) displacement distribution; (b) partial enlargement

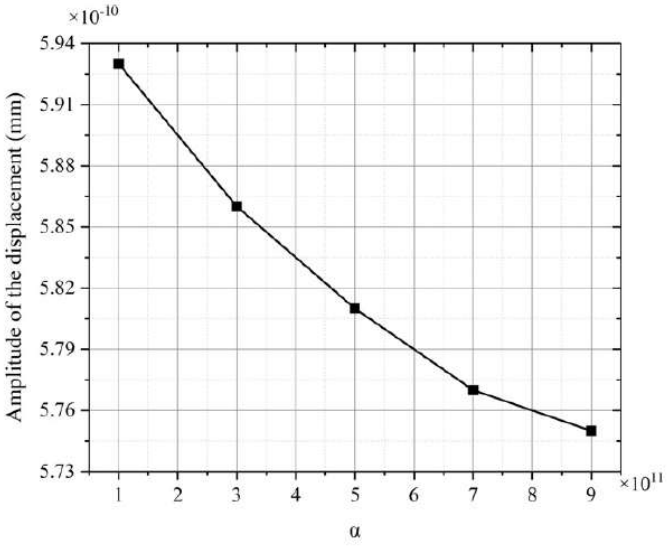

Fig. 13. The amplitude of the displacement with different α

Figure 17(a,b) show the relationship between the aperture angle and the normalized amplitude. The consistency between the experimental results and the simulation results was verified. The size of the aperture angle is approximately linear with the normalized amplitude of the signal except

for one experimental point at an aperture angle of 90°, which is the error in the measurement. It can be concluded through the experiments that the increase in the aperture angle leads to an increase in the focusing intensity, and the signal intensity of the unilateral point-focusing EMAT is 50%–70% larger than that of bilateral one. Therefore, the aperture angle should be set as large as possible.

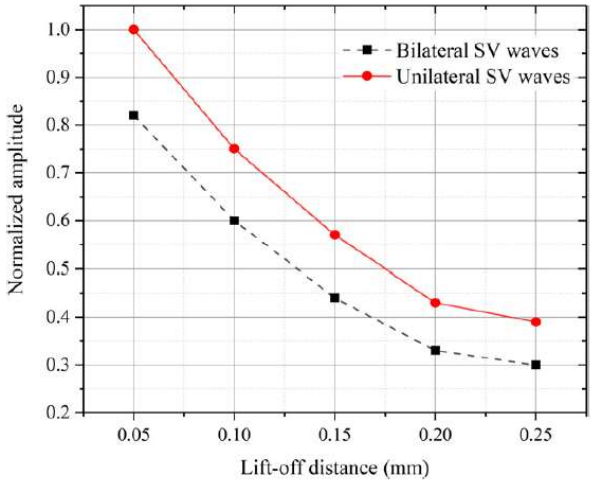

Fig. 14. Normalized amplitude of the displacement field at different life-off distances

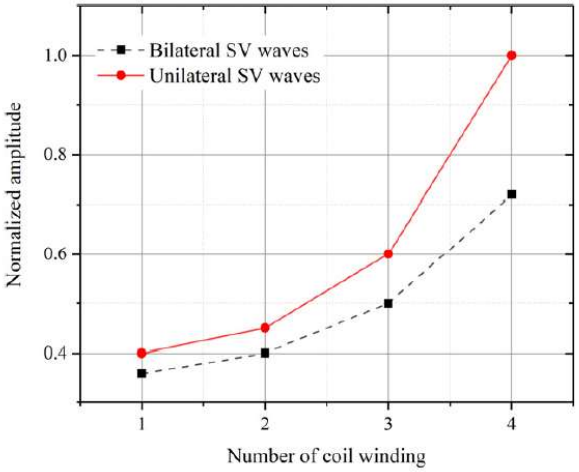

Fig. 15. Normalized amplitude of the displacement field at different coil winding number.

After verifying the effect of the aperture angle on the normalized signal amplitude, Figure 18(a,b) represent the experimental results of the normalized amplitude at different excitation

currents. The amplitude and phase of the voltages generated by the power will affect the amplitude and the phase of the excitation currents in the coils. Experimental results show that the increase in the amplitude of the excitation currents leads to a higher amplitude of the signal, which is similar to simulation results except for some oscillations. The comparison between the normalized amplitude of unilateral and bilateral focusing EMATs shows that the newly designed focusing EMAT has higher signal intensity (60% higher than the traditional bilateral one).

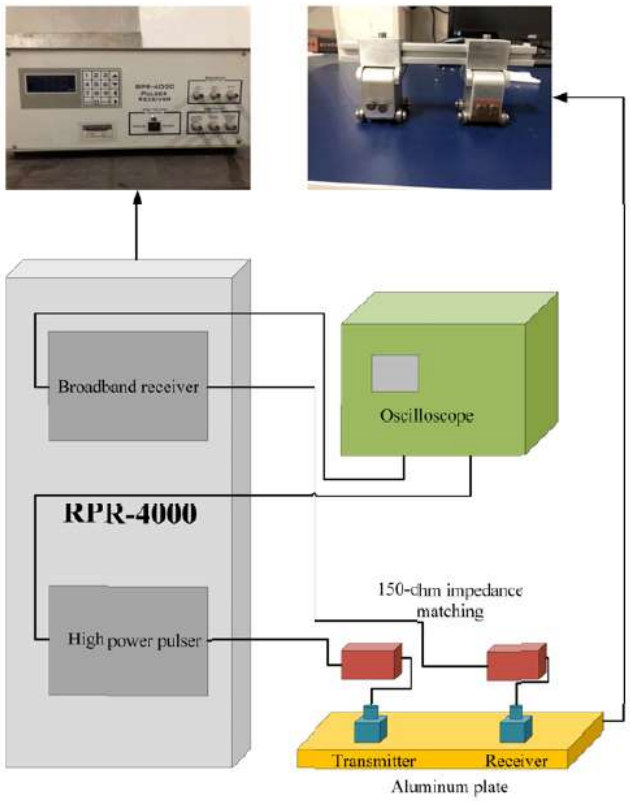

Fig. 16. Experimental setup for the point-focusing EMAT.

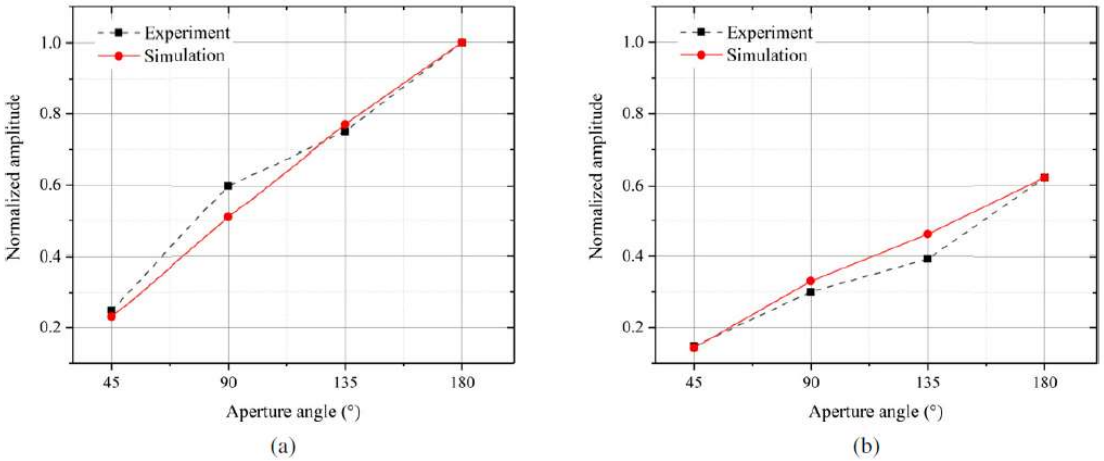

Fig. 17. Experimental verification of the relationship between the aperture angle and the normalized amplitude for: (a) unilateral point-focusing EMAT; (b) bilateral point-focusing EMAT. The normalized amplitude for bilateral point-focusing EMAT is based on the maximum value of the unilateral point-focusing EMAT.

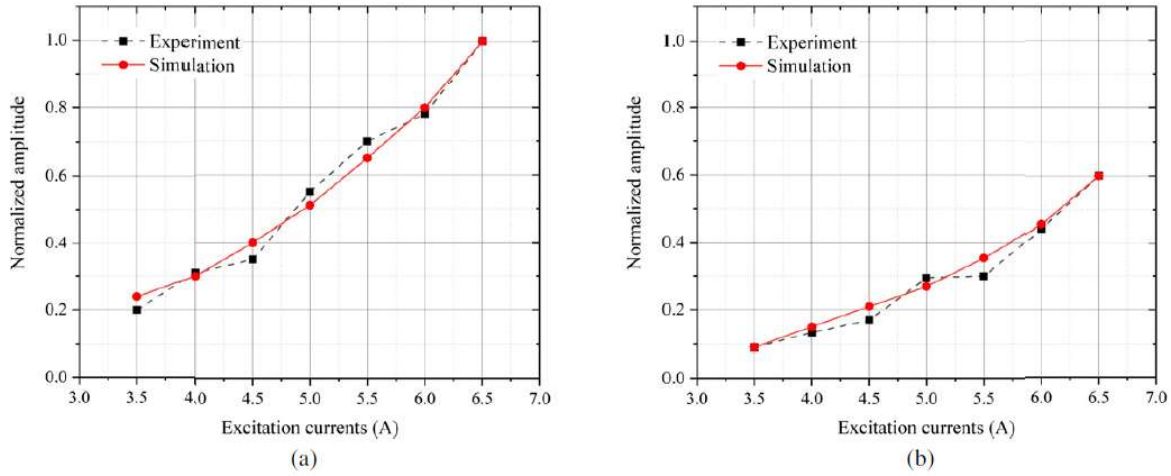

Fig. 18. Experimental verification of the relationship between the excitation current and the normalized amplitude for: (a) unilateral point-focusing EMAT; (b) bilateral point-focusing EMAT. The normalized amplitude for bilateral point-focusing EMAT is based on the maximum value of the unilateral point-focusing EMAT.

6. Conclusions

In this work, Maxwell equations and the wave equation are utilized to calculate the physical process of electromagnetic acoustic transducers (EMATs). Curved meander line coils with a 90° phase difference of the exciting currents have been designed for the unilateral point-focusing EMATs. The focusing intensities of the unilateral and bilateral point-focusing EMATs are verified by both simulation and experiment. It is proved that the unilateral point-focusing EMAT has a better focusing ability of the signal intensity. The effect of the parameters on the focusing capability has been studied in the manuscript.

The increase of the aperture angle, excitation current, and the coil winding number will increase the amplitude of the signal, while the increase of the lift-off distance will reduce it. The focal position also has a significant influence on the intensity of the signal. The oblique incident properties and energy concentration properties of the SV waves lead to the nonlinear relationship between the focal position and the signal amplitude. For the newly designed unilateral point-focusing EMAT, the signal intensity has been proved to be 50%–70% higher than that of a traditional bilateral EMAT under the same conditions; thus the detection accuracy and sensitivity of an EMAT can be improved using an effective unilateral focusing method.

Acknowledgments

This research was supported by the National Key R&D Program of China (Grant No. 2018YFC0809002), National Natural Science Foundation of China (NSFC) (No. 51677093) and Natural Science Foundation of China (NSFC) (No.51777100).

References

[1] [1] X. Jian, L. Baillie, S. Dixon et al., *Journal of Physics D: Applied Physics* **40** (2007), 1501.

[2] X. Jian, S. Dixon, L. Baillie et al., *Journal of Physics D: Applied Physics* **40** (2007), 300.

[3] R.S. Edwards, S. Dixon and X. Jian, *Journal of Physics D: Applied Physics* **37** (2004), 2291.

[4] P. Carr, *IEEE Trans. Microwave Theory Tech* **17** (1969), 845.

[5] H. Ogi, M. Hirao, T. Honda et al., *Transactions of the Japan Society of Mechanical Engineers* **98** (1995), 1191.

[6] H. Ogi, *J. Appl. Phys.* **82** (1997), 3940.

[7] B. Liang, G. Zhai, K. Wang et al. *IEEE Prognostics and System Health Management Conference 1*, 2017.

[8] R. Jafarishapoorabadi, A. Konrad and A. Sinclair, *J. Appl. Phys.* **97** (2005), 2081.

[9] W.J. Pardee and R.B. Thompson, *J. Nondestruct. Eval* **1** (1980), 157.

[10] K. Mirkhani, C. Chaggares, C. Masterson et al., *Ndt & E International* **37** (2004), 181.

[11] R. Ludwig, *IEEE Trans. Ultrason Ferr.* **39** (1992), 476.

[12] T.J. Moran and R.M. Panos, *J. Appl. Phys.* **47** (1976), 2225.

[13] Y.K. Ahn, H.J. Lee and Y.Y. Kim, *Sci. Rep* **7**(1) (2017), 10072.

[14] A. Colombi, V. Ageeva, R.J. Smith et al., *Sci. Rep.* **7** (2017), 6750.

[15] R.B. Thompson, *Appl. Phys. Lett.* **34** (1979), 175.

[16] Z. Wei, S.L. Huang, S. Wang et al., *IEEE Sens. J.* **15** (2015), 6549–6558.

[17] C.B. Thring, Y. Fan and R.S. Edwards, *Ndt & E International* **88** (2017), 1.

[18] C.B. Thring, Y. Fan and R.S. Edwards, *Ndt & E International* **81** (2016), 20.

[19] H. Ogi, M. Hirao and T. Ohtani, *J. Acoust. Soc. Am.* **103** (1998), 2411.

[20] H. Ogi, M. Hirao and T. Ohtani, *IEEE Trans. Ultrason Ferr.* **46** (1999), 341.

[21] K. Ashida, T. Takishita, N. Nakamura, H. Ogi and M. Hirao, *J. JSNDI* **65** (2016), 79.

[22] N. Nakamura, K. Ashida, T. Takishita et al., *Ndt & E International* **83** (2016), 88.

[23] T. Takishita, K. Ashida, N. Nakamura, H. Ogi and M. Hirao, *Jpn. J. Appl. Phys.* **54** (2015), 07HC04.

[24] R. Dhayalan and K. Balasubramaniam, *Ndt & E International* **43** (2010), 519.

[25] X. Jian, S. Dixon, K.T.V. Grattan et al., *Sens. Actuators A.* **128** (2006), 296.

[26] R.B. Thompson, *IEEE Trans. Sonics Ultrason* **SU-25** (1978), 7.

[27] S. Soua, A. Raude and T. Gan, *Proceed-ings of the COMSOL Conference*, 2009.

[28] R. Ludwig and X. Dai, *J. Appl. Phys.* **69** (1991), 89.

[29] K. Kawashima, *J. Acoust. Soc. Am.* **60** (1976), 1089.

[30] R. Dhayalan and K. Balasubramaniam, *Nondestr. Test. Eval.* **26** (2011), 101.

[31] S. Wang, S.L. Huang, Y. Zhang et al., *IEEE Sens. J.* **16** (2016), 6641.

[32] X.J. Jia and Q.Y. Qi, *J. Acoust. Soc. Am.* **143** (2018), 2892.

[33] S. Wang, R. Su, X. Chen et al., *IEEE Trans. Ultrason Ferr.* **60** (2013), 2657.

[34] D. Zhang, Z. Zhou, J. Sun, E. Zhang, Y. Yang and M. Zhao, *IEEE Trans. In-strum. Mea.* **63** (2014), 3058.

[35] G. Miller and H. Pursey, *Proc. R. Soc. London* **223** (1954), 521.